

Discriminating chaotic and integrable regimes in quenched field Floquet system using saturation of Out-of-time-order correlation

Rohit Kumar Shukla,^{1,2,*} Gaurav Rudra Malik,^{3,†} S. Aravinda,^{4,‡} and Sunil Kumar Mishra^{3,§}

¹*Optics and Quantum Information Group, The Institute of Mathematical Sciences,
CIT Campus, Taramani, Chennai 600113, India*

²*Homi Bhabha National Institute, Training School Complex, Anushakti Nagar, Mumbai 400085, India*

³*Department of Physics, Indian Institute of Technology (Banaras Hindu University), Varanasi - 221005, India*

⁴*Department of Physics, Indian Institute of Technology Tirupati, Tirupati, India 517619*

(Dated: April 8, 2024)

The dynamic region of out-of-time-ordered correlators (OTOCs) is a valuable discriminator of chaos in classical and semiclassical systems, as it captures the characteristic exponential growth. However, in spin systems, it does not reliably quantify chaos, exhibiting similar behavior in both integrable and chaotic systems. Instead, we leverage the saturation behavior of OTOCs as a means to differentiate between chaotic and integrable regimes. We use integrable and nonintegrable quenched field Floquet systems to describe this discriminator. In the integrable system, the saturation region of OTOCs exhibits oscillatory behavior, whereas, in the chaotic system, it shows exact saturation *i.e.*, system gets thermalized. To gain a clearer understanding of the oscillations, we calculate the inverse participation ratio (IPR) for the normalized Fourier spectrum of OTOC. In order to further substantiate our findings, we propose the nearest-neighbor spacing distribution (NNSD) of time-dependent unitary operators. This distribution effectively differentiates chaotic and regular regions, corroborating the outcomes derived from the saturation behavior of OTOC.

I. INTRODUCTION

Studying quantum dynamics in many-body systems has been an exciting and challenging frontier in modern physics. Understanding the intricate behavior of quantum correlations, entanglement, and chaos across all dynamical regimes is essential for unlocking the full potential of quantum technologies and shedding light on fundamental aspects of quantum mechanics.

For the class of chaotic dynamics, pioneering research by Larkin and Ovchinnikov delved into the examination of out-of-time-order correlations (OTOCs) as a semiclassical approach to theoretically understand superconductivity[1]. Their study relates the sensitivity of classical trajectories towards the initial conditions to an exponential growth of OTOC. Since then, the concept of OTOC has emerged as a powerful tool to explore the scrambling of information, quantum chaos, butterfly effect [2–12], and phase transition [13–15], providing information about the chaotic nature of the classical and semiclassical systems [2, 3]. A notable development in this field is the recent proposal of a quantum information diode that harnesses OTOC [16]. The exponential growth of OTOC represents the chaotic nature of the systems with a classical analogue, with its exponent being proportional to the Lyapunov exponent[4]. However, it is not conversely true as despite the exponential growth of OTOC, the system in question may be integrable [17].

Recently, researchers have utilized the norm of the adiabatic gauge potential to regulate the adiabatic transitions between eigenstates, revealing its effectiveness as a remarkably sensitive indicator of quantum chaos [18].

The growth of OTOC's has been extensively explored in various spin systems, including Luttinger liquids [19], the XY model [20], the Sachdev-Ye-Kitaev (SYK) model [21], the Heisenberg model, the XXZ model [22, 23], integrable transverse field Ising model (TFIM) [24], integrable and nonintegrable Floquet system [25]. Numerous experimental approaches for measuring OTOC have been proposed in the literature, spanning a wide range of platforms such as cold atoms, cavity and circuit quantum electrodynamics (QED), and trapped-ion simulations [11, 12, 26, 27]. These ideas have paved the way for successful experimental realizations using various systems, such as nuclear spins of molecules [9, 14], trapped ions [28, 29], and ultra-cold gases [30]. It is essential to highlight that the observed behavior consistently demonstrates the power-law growth of the OTOCs in both integrable and chaotic spin systems [25, 31]. This implies that the dynamic region of OTOC does not allow for the differentiation between integrable and chaotic spin systems, as it is limited by the finite-dimensional Hilbert space.

The OTOC is frequently discussed in reference to the Floquet spin Hamiltonian driven by time-periodic fields. [25, 31, 32]. The dynamic and saturation characteristics of OTOCs using the nonlocal spin block observables considering the Floquet Ising model subjected to constant magnetic fields, encompassing both integrable and non-integrable cases, have been studied[25]. Notably, the observed behavior of OTOCs in both integrable and chaotic Floquet systems revealed an approximately quadratic power-law growth pattern. If we consider local spin ob-

* rohitshukla@imsc.res.in

† gauravrudramalik.rs.phy22@iitbhu.ac.in

‡ aravinda@iittp.ac.in

§ sunilkam.app@iitbhu.ac.in

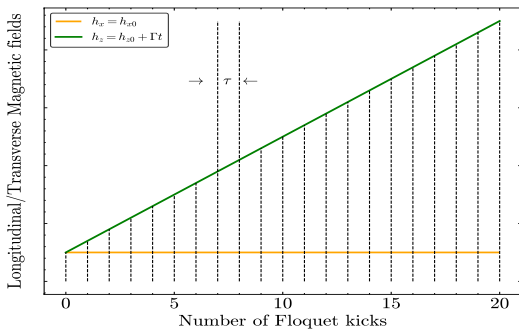


FIG. 1: Illustration of linear quenched field. Transverse magnetic fields are applied in the form of linear with slope Γ and intercept h_{z0} . Kicks are applied after a time interval τ . A constant longitudinal magnetic field of amplitude h_{x0} is applied.

servables, the OTOCs still exhibited a power-law growth in their dynamic region in both integrable and chaotic cases[31]. Consequently, we can say that OTOC in constant fields Floquet system calculated by using different types of observables like single spin observables [31], spin block observables [25], and extensive sums of local observables [32], does not provide exponential growth of OTOC irrespective of the system being chaotic.

Building upon the aforementioned literature, we extend the study of OTOC in the quenched field Floquet system. Here, the ‘quench’ process is performed by varying the magnetic field parameters in time. For this purpose, we chose a simple quench protocol, where the magnetic field is linearly dependent on time. This is referred to as the linear quench protocol. For comparison, we also present results for a case where the applied magnetic fields are given by a sinusoidal function of time in the appendix. The latter model is referred to as the periodic quench protocol. In these conditions for the applied magnetic fields, we will analyze the dynamic and saturation behavior of OTOC using block spin observables as operators. The growth and saturation of OTOC are also discussed in the presence and absence of longitudinal fields, corresponding to nonintegrable and integrable dynamics.

This manuscript is structured as follows. In Section II, we introduce a theoretical framework for the quenched-field Floquet spin Hamiltonian and the corresponding unitary operator. Section III is dedicated to defining OTOCs and block spin observables. In Section IV, we define NNSD within quenched Floquet systems. Section V is where we present the outcomes derived from our simulations. We conclude our findings, highlighting our principal contributions in Section VI.

II. FLOQUET MODEL AND QUENCHED FIELDS

We consider an Ising chain of length N with open boundary conditions, where the quantum spins are described by Pauli matrices σ_i^x , σ_i^y , and σ_i^z . We apply a time-dependent transverse magnetic field with a magnitude h_z that varies like a straight line with slope Γ and intercept h_{z0} . A small constant longitudinal magnetic field of amplitude h_{x0} is also applied. In this transverse direction, kicks are applied with an amplitude given by the linear function at time $t = n\tau$, where n is an integer, and τ is the period of the applied kicks. An illustration of the aforementioned field is depicted in Fig. 1. A system with a time-dependent drive in the form of kicks is called a quenched-field Floquet system. The Hamiltonian of the system is defined as follows:

$$\hat{H}(t) = J\hat{H}_{xx} + h_x\hat{H}_x + h_z(t) \sum_{n=-\infty}^{\infty} \delta\left(n - \frac{t}{\tau}\right)\hat{H}_z. \quad (1)$$

Here, J represents the interaction strength between neighboring spins, h_x is the longitudinal field, and h_z is the transverse field. $\hat{H}_{xx} = \sum_{l=1}^{N-1} \hat{\sigma}_l^x \hat{\sigma}_{l+1}^x$ is the nearest-neighbor Ising interaction term, $\hat{H}_z = \sum_{l=1}^N \hat{\sigma}_l^z$ is the total transverse magnetization, and $\hat{H}_x = \sum_{l=1}^N \hat{\sigma}_l^x$ is total longitudinal magnetization.

The quantum map is the time evolution operator that evolves the system between $n\tau^+$ and $(n+1)\tau^+$ where τ^+ indicates the time just after τ . The quantum map for the quench protocol is given by $\hat{\mathcal{U}}_{xl}(n)$ and defined as (which will be called as \mathcal{U}_{xl} system hereafter)

$$\hat{\mathcal{U}}_{xl}(n) = \left[\prod_{l=1}^N \exp\left(-i\tau\hat{\sigma}_l^x \hat{\sigma}_{l+1}^x - i\tau h_x \hat{\sigma}_l^x\right) \right] \left[\prod_{l=1}^N \exp(-i\tau h_z(n\tau)\hat{\sigma}_l^z) \right]. \quad (2)$$

Under the unitary time evolution, the dynamics of quantum systems cause a spreading of the operators. In the quenched field Floquet system, we consider discrete time evolution. Time evolution operator after n number of kicks defined as $\hat{W}(n) = \hat{U}(n)\hat{W}(0)\hat{U}(n)^\dagger$, where $\hat{U}(n)$ is discrete time evolution of operator and defined as $\hat{U}(n) = \hat{\mathcal{U}}_{xl}(n) \cdots \hat{\mathcal{U}}_{xl}(2)\hat{\mathcal{U}}_{xl}(1)$.

In our analysis, we consider two different types of quenching. First, we examine the simplest case where the transverse fields vary with time and are represented by a straight line with slope Γ and intercept h_{z0} . The expression for the straight line is given by $h_z(t) = h_{z0} + \Gamma t$. In the perpendicular direction, kicks are applied at regular time intervals τ . To induce nonintegrability, we apply a constant longitudinal field with amplitude h_{x0} . In this scenario, the unitary operator is given by $\hat{\mathcal{U}}_{xl}$ in the presence of both longitudinal and transverse fields. When the longitudinal field is absent ($h_{x0} = 0$), the quantum map

is denoted as $\hat{\mathcal{U}}_{0l}$. Here, we use the subscript l with the unitary operator to indicate that the transverse field is applied ‘linearly’. Next, we consider a more complex case where the transverse magnetic field is applied as a cosine wave, and the longitudinal magnetic field is applied as a sine wave. When a periodic field is applied in the system, we refer to it as a periodic quenched field Floquet system. Corresponding to these cases, we denote the unitary operation by $\hat{\mathcal{U}}_{xp}$ and $\hat{\mathcal{U}}_{0p}$ for the integrable and nonintegrable cases, respectively, and use the subscript p to indicate ‘periodicity’. The results of this case are discussed in detail in Appendix A and B with different observables. The periodic quench protocol differs significantly from the linear quench in that the longitudinal field is also time-dependent in the former. However, we do observe a common feature in both quench protocols related to the short- and long-time behavior of the OTOC.

III. OUT-OF-TIME-ORDER CORRELATION

Consider two observable Hermitian commutators $\hat{W}(0)$ and $\hat{V}(0)$. Observable \hat{W} gets time to evolve under Heisenberg time evolution as $\hat{W}(n) = \hat{U}\hat{W}(0)\hat{U}^\dagger$ and observable \hat{V} remains at time $t = 0$. After the time evolution of observable \hat{W} , it displays noncommutativity with $\hat{V}(0)$ which provides the dynamics of the quantum systems by the spreading of operators under the system’s unitary time evolution. This noncommutativity may capture chaotic behavior in the system, which is widely known as OTOC. In mathematical form, OTOC is defined as [1, 25]

$$C(n) = -\frac{1}{2d_A d_B} \text{Tr} \left([\hat{W}(n), \hat{V}]^2 \right), \quad (3)$$

We only consider the situation of equal blocks, $d_A = d_B = 2^{N/2}$ that are dimensions of the subspaces. After doing a trivial calculation, we get $C(n) = \text{Tr}[C_2(n)] - \text{Tr}[C_4(n)]$. $C_2(n)$ and $C_4(n)$ are known as two-point and four-point correlations, respectively, and defined as

$$C_2(n) = -\frac{1}{d_A d_B} \text{Tr} \left(\hat{W}^2(n) \hat{V}^2 \right), \quad (4)$$

$$C_4(n) = -\frac{1}{d_A d_B} \text{Tr} \left(\hat{W}(n) \hat{V} \hat{W}(n) \hat{V} \right). \quad (5)$$

The OTOC quantifies how much the commutator of these operators at different times grows as a function of time. In chaotic systems, the OTOC typically grows exponentially with time, which is a signature of quantum chaos. This exponential growth of OTOC is often referred to as the ‘butterfly effect’, where small variations at one point in a quantum system can lead to significantly different outcomes at a later time, making long-term predictions of quantum behavior highly sensitive to initial conditions.

Spin Block Observables: Let us consider a chain of length N (N should be even) and divide it into two halves blocks. The first block is defined as observable \hat{W} and the second block is defined as observable \hat{V} . These observables are named spin block observables (SBOs). In the mathematical form, these are defined as:

$$\hat{W} = \frac{2}{N} \sum_{l=1}^{\frac{N}{2}} \hat{\sigma}_l^x \quad \text{and} \quad \hat{V} = \frac{2}{N} \sum_{l=\frac{N}{2}+1}^N \hat{\sigma}_l^x \quad (6)$$

Note that SBOs \hat{W}_B and \hat{V}_B are Hermitian but nonunitary. Due to this, $C_2(n)$ is not reduced to unity and effectively results in $C(\infty) = 4/N^2$ [25]. The motivation for considering SBOs is to increase the dimension of the Hilbert space of the observables compared to single-site observables. Additionally, SBOs remove the characteristic region of the OTOC, allowing for more rapid saturation. Our focus here is on the saturation behavior of the OTOC, and therefore, we restrict the characteristic regime of the OTOC by choosing spin block observables.

IV. NEAREST-NEIGHBOUR SPACING DISTRIBUTION

The nearest-neighbor spacing distribution (NNSD) is a concept commonly used in the field of chaos and random matrix theory to study the statistical properties of energy levels of complex systems [33–36]. It provides insights into the level repulsion and clustering behavior of eigenvalues in such systems. The NNSD is therefore particularly relevant when studying systems with chaotic and regular dynamics as it characterizes the distribution of spacings between adjacent energy levels, distinguishing a chaotic system from an integrable one [37, 38].

In the context of quantum mechanics, the Hamiltonian plays a crucial role in describing the statistical properties of the energy levels of a quantum system. However, when dealing with time-dependent Hamiltonians, such as those encountered in Floquet systems, the situation becomes more complex. In the Floquet theory, systems are subject to periodic driving, and the Hamiltonian is explicitly time-dependent. This time dependence often leads to challenges in finding exact analytical solutions, especially when there are Dirac delta function terms or other discontinuities present in the Hamiltonian. For such cases, another approach exists, which involves the spectral analysis of the corresponding unitary operator for one period [25]. In a Floquet system, unitary operators exhibit similar behavior after a period of kicks *i.e.*, $\hat{\mathcal{U}}_x(t + \tau) = \hat{\mathcal{U}}_x(\tau)$. The spectral statistics of the system can be fully characterized by the unitary operator for a single period. This spectral analysis involves decomposing the unitary operator into its eigenvalues and eigenvectors, just as in the time-independent case [25].

In a quenched field Floquet system, where the amplitude of the field changes with time, the unitary operators

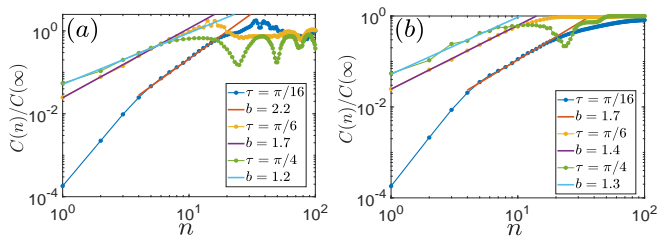


FIG. 2: $C(n)/C(\infty)$ vs n for (a) integrable $\hat{\mathcal{U}}_{0l}$ ($h_{x0} = 0$) (b) nonintegrable $\hat{\mathcal{U}}_{xl}$ system ($h_{x0} = 1$) for period $\tau = \pi/16$, $\pi/6$, and $\pi/4$. The parameters used for the numerics are $J = 1$, $h_{z0} = 1$, $\Gamma = 0.1$ and $N = 12$. b is the power exponent *i.e.*, $C(n)/C(\infty) \sim n^b$. The open boundary condition is considered.

for different periods can indeed be different. This implies that the unitary operator depends on the time ordering of the kicks. As a result, we cannot explain the spectral statistics of the system by using the unitary operator for just one period, as we can in a constant field Floquet system. To describe the spectral statistics of the system in a quenched field Floquet system, we need to consider the unitary operator for all the individual kicks. For example, if we want to find the spectral statistics at first, second, and third kicks, we would consider the following unitary operators $\hat{U}(1) = \hat{\mathcal{U}}_x(1)$, $\hat{U}(2) = \hat{\mathcal{U}}_x(2)\hat{\mathcal{U}}_x(1)$, and $\hat{U}(3) = \hat{\mathcal{U}}_x(3)\hat{\mathcal{U}}_x(2)\hat{\mathcal{U}}_x(1)$, respectively. We would then calculate the spectral statistics of each of these unitary operators individually to describe the spectral statistics at these three different kicks. If we are interested in the spectral statistics over a larger number of kicks, we would follow a similar process by considering the corresponding unitary operators for each kick.

In calculating the NNSD, it is essential to eliminate the symmetries present in the system to remove degeneracy. Floquet system with open boundary conditions possesses reflection symmetry. This can be removed by generating Hamiltonian by only even Palindromic eigenvector (for details, see the Ref. [25]). We then calculate the differences between consecutive eigenvalues of the Hamiltonian generated by even Palindromic sequences. These differences are computed in the form of ensembles denoted as s . After obtaining the ensemble of s , we can draw the distribution of these ensembles. This distribution is known as NNSD. If the NNSD closely adheres to the Wigner-Dyson (WD) distribution, the system exhibits strong chaotic behavior. The WD distribution is mathematically expressed as [33, 39]:

$$P_W(s) = \frac{\pi s}{2} e^{-\pi s^2/4}. \quad (7)$$

Conversely, if the NNSDs exhibit Poisson statistics, the system is termed nontrivially integrable. The Poisson distribution is given by:

$$P_P(s) = e^{-s}. \quad (8)$$

V. RESULTS

We study the OTOC in linearly quenched Floquet systems, examining both integrable and nonintegrable scenarios. To enhance the dimensionality of the observable's Hilbert space, we employ SBOs in our calculations. Our objective is to identify key distinctions between integrable and chaotic systems. We analyze the dynamic and saturation regions of the OTOC to achieve this goal. To justify chaotic behavior as defined by the OTOC, we calculate the NNSD for a time-dependent unitary operator.

Under the linear quench our Floquet system introduces an approximately quadratic exponent in the power-law growth of OTOCs in both integrable [Fig. 2(a)] and nonintegrable systems [Fig. 2(b)] for a small period *i.e.*, $C(n)/C(\infty) \sim n^b$ where $b \approx 2$, b is known as the power exponent. As the period of the transverse kicks increases, we observe a decrease in the associated exponent of the power law growth. This contrasts with the behavior of the equivalent nonintegrable system under a constant field, where a longer Floquet period leads to an increase in the power law exponent [25]. In the current scenario, there is a time-dependent transverse magnetic field. As the period increases, the transverse kick amplitude becomes rapidly dominant due to its magnitude being defined by $h_z(n\tau) = h_{z0} + n\tau\Gamma$ and thermalizes the system in a shorter number of kicks. This in turn leads to a suppression in the growth exponent.

The initial goal of identifying exponential growth in the chaotic system before the scrambling time sought to provide a distinguishing factor between integrable and chaotic systems. However, the emergence of power-law growth across both scenarios shifted our attention to a new line of inquiry. Instead of focusing on growth, we turned our gaze towards saturation behavior that could potentially serve as a powerful discriminator. As we delve into the saturation behavior of OTOCs, a promising avenue unfolds. Our exploration now centers on how OTOCs saturate—does this behavior differ between integrable and chaotic systems? Can it offer a unique lens through which to distinguish between these two complex regimes? The investigation into the saturation behavior of OTOCs holds immense potential. By meticulously observing how OTOCs saturate, we aim to uncover distinctive patterns that could serve as robust indicators of system behavior. Whether integrable systems showcase different saturation behavior compared to chaotic counterparts is a question that drives our exploration forward.

We investigate the saturation behavior of the OTOC in a linearly quenched Floquet system. By studying the OTOC's behavior in the long-time regime, we aim to distinguish between signatures of integrable and chaotic dynamics. We specifically explore three different periods: $\tau = \pi/16$, $\tau = \pi/6$, and $\tau = \pi/4$. We choose $\tau = \pi/16$ for its small size, $\tau = \pi/6$ for its larger size, and $\tau = \pi/4$ as it represents a special point in the Floquet case, showing periodic behavior of OTOC [25]. However, in

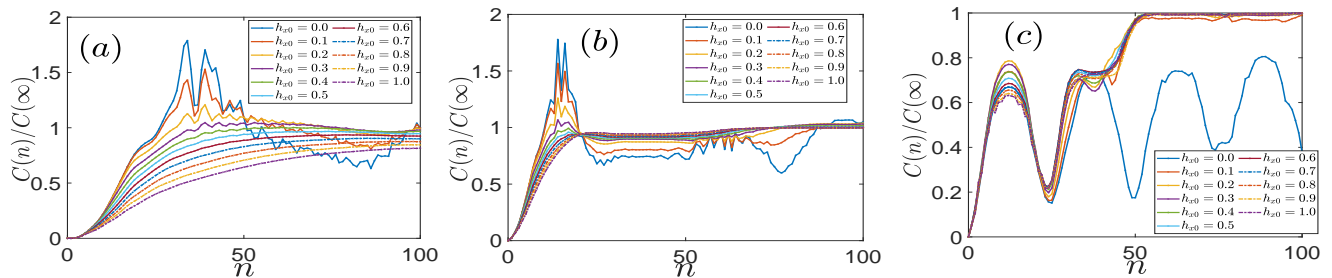


FIG. 3: $C(n)/C(\infty)$ vs n for different value of h_{x0} lies in between 0 to 1 differing by 0.1 for nonintegrable $\hat{\mathcal{U}}_{xl}$ system at period (a) $\tau = \pi/16$, (b) $\tau = \pi/6$, and (c) $\tau = \pi/4$. Other parameters are: $J = 1$, $h_{z0} = 1$, $\Gamma = 0.1$, and $N = 12$. Open boundary conditions are considered.

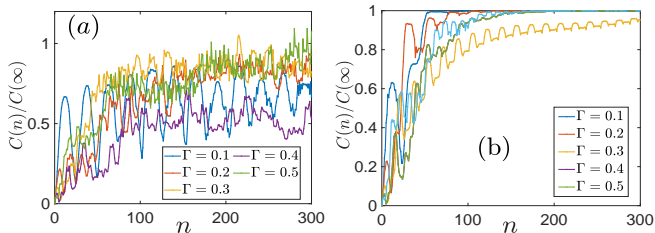


FIG. 4: $C(n)/C(\infty)$ vs n for (a) integrable $\hat{\mathcal{U}}_{ol}$ and (b) nonintegrable $\hat{\mathcal{U}}_{xl}$ system with period $\tau = \pi/4$ at different value of Γ . Other parameters are: $J = 1$, $h_{x0} = 0/1$, $h_{z0} = 1$, and $N = 12$. Open boundary conditions are considered.

the quenched case, it does not exhibit periodic behavior due to the constant (h_x/h_z) being multiplied by the period $\pi/4$, unlike the special case where $h_x = h_z = 1$. We study the saturation behavior at all three periods by varying the longitudinal field from 0 to 1 in increments of 0.1. This approach helps us understand the effect of chaos in the saturation region of the OTOC. When the nonintegrability term is absent, oscillations are present in the OTOC behavior for all periods. However, as we introduce a small nonintegrability term, the oscillation amplitude decreases, and after a certain value of h_{x0} , it saturates at a specific value [Fig. 3 (a–c)]. At the period $\tau = \pi/4$, we observe exact saturation in the long-time regime of the OTOC with the introduction of a small nonintegrability term [Fig. 3 (c)]. The exact saturation of the OTOC signifies the complete thermalization of the system, indicating the chaotic behavior of its underlying dynamics. Hence, it is proposed that a specific value of the nonintegrability term drives the system into chaos.

The oscillation behavior of OTOCs decreases when introducing and increasing the chaotic term in the system. Additionally, the saturation behavior depends on the growth rate of the linear quench. The shift from oscillatory to stationary behavior is sustained when transitioning from the integrable to the chaotic dynamic class for various Γ values, as shown in Fig. 4. Since the integrable to chaotic transition is based on the absence or presence of the constant longitudinal field term, we can

claim that the broad nature of oscillatory versus stationary behavior for the OTOC is largely independent of the strength of the applied quench. To understand the effect of the applied quench on the saturation region of the OTOC, a quantitative analysis is necessary. For this purpose, we calculate the inverse participation ratio, as discussed below.

Inverse Participation Ratio: We will calculate the inverse participation ratio (IPR) to describe the oscillation behavior in the saturation region of OTOC. The IPR studies are useful in characterizing the localization in a many-body system. The IPR is defined for a many-body eigenstate $|\psi_i\rangle$ in the basis $\{\phi_j\}_{j=1}^{j=D}$ written as $|\psi_i\rangle = \sum_j a_{ij} |\phi_j\rangle$ [40]:

$$\xi(i) = \left[\sum_{j=1}^{j=D} |a_{ij}|^4 \right]^{-1}. \quad (9)$$

A small (large) value of $\xi(i)$ (min. value = 1) indicates the presence of a few (many) basis states in the superposition to form the wave function. Thus, large value of $\xi(i)$ indicates delocalization of the quantum state [41–43].

A similar approach can be used for a normalized Fourier spectrum corresponding to the OTOC values. In the Floquet system, the OTOC values form a discrete time series like C_k , where C_k represents the value of the OTOC at time $k * \tau$ with integer k and period τ . This may be converted into f_j ($j \in \mathbb{Z}^+$) by the discrete Fourier transform. Following normalization where $\sum_{j=1}^D |f_j|^2 = 1$, we may define:

$$\xi_{OTOC} = \left(\sum_{j=1}^{j=D} |f_j|^4 \right)^{-1}. \quad (10)$$

where D is the dimension of Hilbert space *i.e.*, $D = 2^N$. Similar to $\xi(i)$, a small (large) value of ξ_{OTOC} indicates the presence of a small (large) number of frequency components in the OTOC time series.

We analyze the IPR at the three different τ values: $\pi/16$, $\pi/6$, and $\pi/4$, corresponding to the OTOC behavior depicted in Fig. 3 (a), (b), and (c), respectively. After

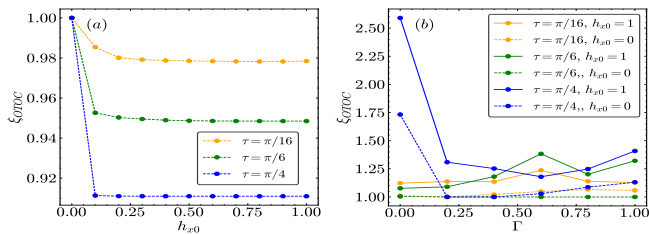


FIG. 5: IPR vs (a) h_{x0} and (b) Γ for integrable $\hat{\mathcal{U}}_{0l}$ system ($h_{x0} = 0$, solid line), and nonintegrable $\hat{\mathcal{U}}_{xl}$ system ($h_{x0} = 1$, dotted line) at three different period $\tau = \pi/16$, $\pi/6$, and $\pi/4$. Other parameters are: $J = 1$, $h_{z0} = 1$ and $N = 12$. Open boundary conditions are considered.

obtaining the values for the IPR, we carry out a normalization wherein we express each entry as a fraction of the maximum IPR value obtained for that particular driving period. This allows for a more effective comparison and enables us to understand the role of the h_{x0} term. Note that the maximum value of the IPR always corresponds to $\Gamma = 0$ for all the driving periods. We observe that the IPR decreases with an increase in h_{x0} and saturates to a fixed value [Fig. 5(a)]. This suggests that compared to the integrable case ($h_x = 0$), where several frequencies contribute to the oscillation, some of these frequencies are removed as we move towards the chaotic regime ($h_x > 0$), for all driving periods. This suggests that the frequencies of oscillation in the saturation region of OTOC has decreased. Additionally, one can see that as the period increases, the IPR value decreases for a given value of h_{x0} .

The saturation behavior of the OTOC in both integrable and chaotic systems depends on the growth rate Γ of the transverse kicking field. This dependence is reflected in the IPR as the Γ value changes. In both integrable and chaotic quenched field Floquet systems, increasing the value of Γ always increases the IPR compared to when $\Gamma = 0$ [Fig. 5(b)]. This indicates that introducing a quench and increasing the growth rate of the quench enhance the oscillatory behavior of the OTOCs compared to a Floquet system with a constant field. Notably, the increase in the integrable cases is much larger than that in the chaotic examples, where the change is virtually negligible [Fig. 5(b)].

An exception to the above is the case for $\tau = \pi/4$, where $\Gamma = 0$ corresponds to the highest value of the IPR. In the quenched field Floquet system, $\Gamma = 0$ corresponds to the constant field Floquet system. The period $\tau = \pi/4$ in the constant field Floquet system represents a special case as discussed in several contexts [25, 44–48]. At this driving period the OTOC exhibits periodic behavior, with the period trivially depends on the system size in the integrable case but nontrivially depends in the nonintegrable case [25]. For other values of Γ , no special characteristics are associated with the $\pi/4$ driving period.

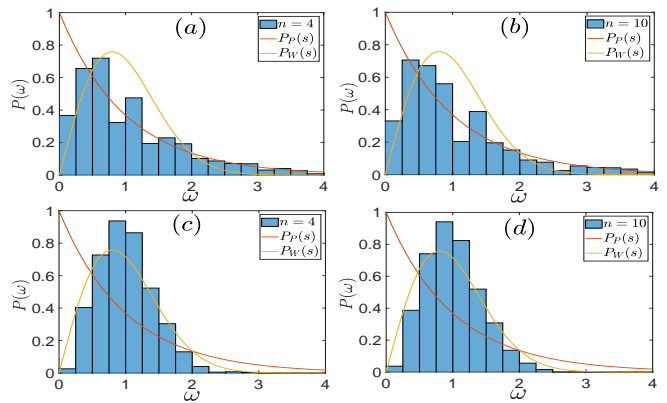


FIG. 6: NNSD of the integrable $\hat{\mathcal{U}}_{0l}$ system (a & b), and nonintegrable $\hat{\mathcal{U}}_{xl}$ system (c & d) at period $\tau = \pi/4$ in the even Palindromic space at different kicks mentioned in the legend. Other parameters are: $J = 1$, $h_{z0} = 1$, $h_{x0} = 0/1$, $\Gamma = 0.1$, and $N = 12$. Open boundary conditions are considered.

Nearest-neighbour-spacing-distribution: In order to further classify the dynamics for our system upon the addition of the integrability breaking longitudinal magnetic field, we obtain the NNSD for our system. In the absence of a classical analogue to our system, we have the NNSD as the strongest indicator of chaotic signatures inherent in our nonintegrable system. Such a signature is manifested by energy level distribution being clustered or separated, for the integrable and chaotic/nonintegrable dynamics. The spectral statistics, typically associated with stationary systems, encapsulate valuable information about energy level distributions and correlations within a quantum spectrum. We extend this exploration to the realm of time-dependent unitary operators, introducing an entirely new aspect to spectral analysis. The absence of this investigation in the existing literature underscores the novelty of our approach. In the integrable case, the clustered NNSD showcases a Poisson-type distribution [Fig. 6(a – b)]. However, as we transition to the chaotic scenario, a profound shift occurs—the NNSD transforms into a Wigner-Dyson-type distribution [Fig. 6(c – d)], indicating level repulsion. This behavior mirrors the complex and chaotic dynamics intrinsic to chaotic systems, highlighting the emergence of delocalized modes and irregularities.

To extend the universality of our findings in the quenched field Floquet system, we replace the linear transverse magnetic fields with time-periodic fields in both the transverse and longitudinal directions, represented by cosine and sine waves, respectively. In the transverse direction, the fields are applied as kicks, with their amplitudes decreasing over time in a cosine-like fashion. By employing a more sophisticated field configurations, we transform the Floquet system into a periodically quenched field Floquet system. In our calculations of the OTOC, we utilize SBOs as the observable.

Similar to the impact of a linear quenched field, in the case of a periodic quenched field, OTOCs exhibit power-law growth before the scrambling time, with a higher exponent, approximately $b \approx 10$, observed in both integrable and chaotic systems. In this context, the saturation behavior of the OTOC also serves as a distinguishing feature between integrable and chaotic systems. Specifically, in integrable systems, the OTOC displays oscillatory behavior in the saturation regime, while chaotic systems exhibit exact saturation. To validate these findings, we analyze the NNSD of time-dependent unitary operators. The NNSD demonstrates Poisson-like behavior in the integrable case for all kicks. However, in the chaotic case, it transitions to a Wigner-Dyson type of behavior after a fixed number of kicks. These results are elaborated in the Appendix A. Subsequently, we also investigate the saturation behavior of the OTOC using localized spin observables *i.e.*, Pauli spin observables in the x -directions. By repeating our calculations with this observable, we have observed a consistent pattern of saturation behavior. Specifically, the OTOCs display oscillatory behavior in integrable systems, whereas in chaotic systems, they saturate at specific values. A detailed discussion and results for this case can be found in Appendix A.

We also investigate how different observables affect the saturation behavior of the OTOC in periodic quenched field Floquet systems. Specifically, we consider two types of observables. Firstly, we analyze block spin observables where spins are aligned in the z -direction, in contrast to our primary results where spins are aligned in the x -direction. We study the saturation behavior for periods of $\pi/16$, $\pi/6$, and $\pi/4$. Across all cases, we find that the OTOC exhibits exact saturation after a certain number of kicks in chaotic systems, while showing oscillatory behavior in integrable systems. Additional details and results can be found in Appendix B. Furthermore, we consider localized spin observables, *i.e.*, Pauli observables in the z -direction. By repeating our calculations with these observables, we consistently observe a similar pattern of saturation behavior. Specifically, the OTOCs display oscillatory behavior in integrable systems, whereas in chaotic systems, they saturate at specific values. A detailed discussion and results for the localized observables in the z -direction can be found in Appendix B. These findings indicate that in the context of quench dynamics, the saturation behavior of OTOCs can be a powerful discriminator between integrable and chaotic systems.

VI. CONCLUSION

We study the behavior of OTOCs using SBOs for a linear quenched field Floquet system. For the quench, we apply a transverse magnetic field increasing linearly in time with a slope Γ and apply the kicks in a period of τ . We apply a constant longitudinal magnetic field to make the system chaotic. Our focus is on understanding

how these OTOCs evolve in the presence and absence of longitudinal fields, exploring their growth and saturation characteristics. In both the integrable and chaotic cases for the linearly quenched Floquet systems, we observe a common pattern of power-law growth in the OTOCs with quadratic exponent for a small period which decreases as the driving period increases. Intriguingly, when we examine the dynamic region, we find no discernible differences between integrable and chaotic systems. This suggests that the initial dynamics do not discriminate the chaotic properties of the system. To distinguish between integrable and chaotic systems, we turn our attention to the saturation behavior of the OTOCs. Here, we find a key distinction. By analyzing how the OTOCs reach a plateau or saturation point, we uncover a reliable indicator of system behavior. In the integrable system, OTOC provides oscillating behavior in the regime of saturation however chaotic systems display exact stabilisation. The concept of similar behavior of OTOCs is explored in diverse physical systems [40, 49]. To further validate our findings, we employ the calculation of the NNSD. This additional analysis consistently supports our earlier observations, providing robust evidence for the distinction between integrable and chaotic systems. To generalize our findings, we explore a different type of quenching scenario where both longitudinal and transverse fields are time-dependent in the system. Additionally, we consider different types of observables to study their impact on the saturation behavior of the OTOC. Across all scenarios, we consistently observe that the saturation region of the OTOC displays oscillatory behavior in integrable systems, while exhibiting exact saturation in chaotic systems, regardless of the observables used. Detailed results and discussions for these scenarios can be found in Appendices A and B.

The oscillation in the saturation behavior of OTOC is influenced by the growth rate of the transverse field. However, it is not explicitly determined by the OTOC itself. To address this, we investigate the behavior of IPR in the presence and absence of longitudinal fields. In the absence of the longitudinal field the IPR takes its maximum value which decreases and saturates as soon as a longitudinal field is applied. Additionally, we observe that as the period of the system increases, the IPR decreases. Our findings further indicate that as the growth rate Γ increases, the value of the IPR is higher compared to the case of $\Gamma = 0$. At $\tau = \pi/4$ with $\Gamma = 0$, there is an exception in both integrable and chaotic systems because at this point IPR value is very high and is governed by the periodic behavior of OTOC.

In conclusion, our findings suggest that the saturation behavior of the OTOC can serve as a robust indicator to distinguish between integrable and chaotic systems, irrespective of the specific quenching protocol or the choice of observables.

ACKNOWLEDGEMENT

We would like to acknowledge the support provided by the project “Study of quantum chaos and multipartite entanglement using quantum circuits” sponsored by the Science and Engineering Research Board (SERB), Department of Science and Technology (DST), India under

the Core Research Grant CRG/2021/007095. We also acknowledge the computing resources of ‘PARAM Shivay’ at the Indian Institute of Technology (BHU), Varanasi supported by the Centre for Development of Advanced Computing (C-DAC), the Ministry of Electronics and Information Technology (MeitY) and Department of Science and Technology (DST).

-
- [1] A. Larkin and Y. N. Ovchinnikov, *Sov Phys JETP* **28**, 1200 (1969).
- [2] J. Maldacena, S. H. Shenker, and D. Stanford, *Journal of High Energy Phys.* **08**, 106 (2016).
- [3] R. Prakash and A. Lakshminarayan, *Phys. Rev. B* **101**, 121108 (2020).
- [4] E. B. Rozenbaum, S. Ganeshan, and V. Galitski, *Phys. Rev. Lett.* **118**, 086801 (2017).
- [5] I. L. Aleiner, L. Faoro, and L. B. Ioffe, *Annals of Phys.* **375**, 378 (2016).
- [6] D. A. Roberts and B. Swingle, *Phys. Rev. Lett.* **117**, 091602 (2016).
- [7] P. Hosur, X.-L. Qi, D. A. Roberts, and B. Yoshida, *Journal of High Energy Phys.* **02**, 004 (2016).
- [8] Y. Huang, Y.-L. Zhang, and X. Chen, *Annalen der Physik* **529**, 1600318 (2017).
- [9] K. X. Wei, C. Ramanathan, and P. Cappellaro, *Phys. Rev. Lett.* **120**, 070501 (2018).
- [10] N. Abelung, L. Cevolani, and S. Kehrein, *SciPost Physics* **5**, 052 (2018).
- [11] B. Swingle, G. Bentsen, M. Schleier-Smith, and P. Hayden, *Phys. Rev. A* **94**, 040302 (2016).
- [12] N. Y. Yao, F. Grusdt, B. Swingle, M. D. Lukin, D. M. Stamper-Kurn, J. E. Moore, and E. A. Demler, *arXiv preprint arXiv:1607.01801* (2016).
- [13] M. Heyl, F. Pollmann, and B. Dóra, *Phys. Rev. Lett.* **121**, 016801 (2018).
- [14] B. Chen, X. Hou, F. Zhou, P. Qian, H. Shen, and N. Xu, *Applied Phys. Lett.* **116**, 194002 (2020).
- [15] R. K. Shukla, G. K. Naik, and S. K. Mishra, *EPL* **132**, 47003 (2021).
- [16] R. K. Shukla, L. Chotorlishvili, V. Vijayan, H. Verma, A. Ernst, S. S. Parkin, and S. K. Mishra, *Materials for Quantum Technology* **3**, 035003 (2023).
- [17] C.-J. Lin and O. I. Motrunich, *Phys. Rev. B* **97**, 144304 (2018).
- [18] M. Pandey, P. W. Claeys, D. K. Campbell, A. Polkovnikov, and D. Sels, *Physical Review X* **10**, 041017 (2020).
- [19] B. Dóra and R. Moessner, *Phys. Rev. Lett.* **119**, 026802 (2017).
- [20] J.-H. Bao and C.-Y. Zhang, *Communications in Theoretical Phys.* **72**, 085103 (2020).
- [21] W. Fu and S. Sachdev, *Phys. Rev. B* **94**, 035135 (2016).
- [22] J. Riddell and E. S. Sørensen, *Phys. Rev. B* **99**, 054205 (2019).
- [23] J. Lee, D. Kim, and D.-H. Kim, *Phys. Rev. B* **99**, 184202 (2019).
- [24] C.-J. Lin and O. I. Motrunich, *Phys. Rev. B* **97**, 144304 (2018).
- [25] R. K. Shukla, A. Lakshminarayan, and S. K. Mishra, *Phys. Rev. B* **105**, 224307 (2022).
- [26] G. Zhu, M. Hafezi, and T. Grover, *Phys. Rev. A* **94**, 062329 (2016).
- [27] M. Campisi and J. Goold, *Phys. Rev. E* **95**, 062127 (2017).
- [28] K. A. Landsman, C. Figgatt, T. Schuster, N. M. Linke, B. Yoshida, N. Y. Yao, and C. Monroe, *Nature* **567**, 61 (2019).
- [29] M. K. Joshi, A. Elben, B. Vermersch, T. Brydges, C. Maier, P. Zoller, R. Blatt, and C. F. Roos, *Phys. Rev. Lett.* **124**, 240505 (2020).
- [30] E. J. Meier, J. Ang’ong’a, F. A. An, and B. Gadway, *Phys. Rev. A* **100**, 013623 (2019).
- [31] R. K. Shukla and S. K. Mishra, *Phys. Rev. A* **106**, 022403 (2022).
- [32] I. Kukuljan, S. Grozdanov, and T. Prosen, *Phys. Rev. B* **96**, 060301 (2017).
- [33] M. L. Mehta, *Random matrices*, 3rd ed. (Academic Press, Cambridge, MA, 2004).
- [34] L. Santos, *Journal of Physics A: Mathematical and General* **37**, 4723 (2004).
- [35] E. Bogomolny, B. Georgeot, M.-J. Giannoni, and C. Schmit, *Physical review letters* **69**, 1477 (1992).
- [36] O. Bohigas, M.-J. Giannoni, and C. Schmit, *Physical review letters* **52**, 1 (1984).
- [37] Y. Alhassid and R. Levine, *Physical Review A* **40**, 5277 (1989).
- [38] T. Prosen and M. Robnik, *Journal of Physics A: Mathematical and General* **26**, 2371 (1993).
- [39] L. D’Alessio, Y. Kafri, A. Polkovnikov, and M. Rigol, *Advances in Physics* **65**, 239 (2016).
- [40] E. M. Fortes, I. García-Mata, R. A. Jalabert, and D. A. Wisniacki, *Physical Review E* **100**, 042201 (2019).
- [41] G. Misguich, V. Pasquier, and J.-M. Luck, *Physical Review B* **94**, 155110 (2016).
- [42] E. Tsukerman, *Physical Review B* **95**, 115121 (2017).
- [43] B. Kramer and A. MacKinnon, *Rep. Prog. Phys.* **56**, 1469 (1993).
- [44] R. K. Shukla, *arXiv preprint arXiv:2310.14620* (2023).
- [45] S. K. Mishra and A. Lakshminarayan, *Europhysics Lett.* **105**, 10002 (2014).
- [46] S. K. Mishra, A. Lakshminarayan, and V. Subrahmanyam, *Phys. Rev. A* **91**, 022318 (2015).
- [47] A. Lakshminarayan and V. Subrahmanyam, *Phys. Rev. A* **71**, 062334 (2005).
- [48] G. K. Naik, R. Singh, and S. K. Mishra, *Phys. Rev. A* **99**, 032321 (2019).
- [49] J. Novotný and P. Stránský, *Phys. Rev. E* **107**, 054220 (2023).

Appendix A: OTOCs using SBOs and Pauli observables with x -direction alignment in periodic quenched field Floquet systems

Let us discuss a more challenging scenario where both the longitudinal and transverse magnetic fields are time-dependent. Unlike the previous case, here, the longitudinal field varies with time. We use both longitudinal and transverse magnetic fields, represented by sine and cosine functions, respectively. Mathematically, they are described as $h_x = h_{x0} \sin(\alpha t)$ and $h_z = h_{z0} \cos(\alpha t)$. The corresponding Hamiltonian for these time-dependent fields is given by

$$\hat{H}(t) = J\hat{H}_{xx} + h_x(t)\hat{H}_x + h_z(t) \sum_{n=-\infty}^{\infty} \delta\left(n - \frac{t}{\tau}\right)\hat{H}_z \quad (\text{A1})$$

The quantum map is the time evolution operator that evolves the system between $n\tau^+$ and $(n+1)\tau^+$ where τ^+ indicates the time just after τ . The quantum map for the quench protocol is given by $\hat{\mathcal{U}}_{xp}(n)$ and defined as (which will be called as $\hat{\mathcal{U}}_{xp}$ system hereafter)

$$\hat{\mathcal{U}}_{xp}(n) = \left[\prod_{l=1}^N \exp\left(-i\tau\hat{\sigma}_l^x \hat{\sigma}_{l+1}^x - \int_{n\tau}^{(n+1)\tau} h_x(t) dt \hat{\sigma}_l^x\right) \right] \left[\prod_{l=1}^N \exp(-i\tau h_z(n\tau)\hat{\sigma}_l^z) \right]. \quad (\text{A2})$$

Corresponding to the periodic quenched in the transverse direction, we will call the system periodic quenched field Floquet systems and use the notation for the present is $\hat{\mathcal{U}}_{xp}$ and $\hat{\mathcal{U}}_{0p}$ for the nonintegrable and integrable cases, respectively. For the calculation of OTOC, we consider the same SBOs as in the main text SBO *i.e.*, \hat{W}_B and \hat{V}_B . At the initial time, $t = 0$, the operators \hat{W}_B and \hat{V}_B commute. However, immediately after n kicks at $t = n\alpha\tau$, the operator $\hat{W}_B(n) = \left(\prod_{k=1}^n \hat{U}(k)\right)^\dagger \hat{W}_B \left(\prod_{k=1}^n \hat{U}(k)\right)$ loses its commutative property. As time progresses, the envelope of the kicked transverse field gradually decreases from its maximum value h_{z0} due to the cosine function. Concurrently, during the same period, the longitudinal field undergoes an increase from 0 to its maximum value h_{x0} due to the sine functions. The frequency of these fields is held constant at $\alpha = \pi/2t_{\max}$, with t_{\max} denoting the duration of the evolution, and in this context, t_{\max} is taken as 16π .

Similar to the linear quenched field Floquet system, periodic quenched fields Floquet system displays the power-law growth of OTOCs as $C(n)/C(\infty) \sim n^b$ in both integrable and nonintegrable systems [Fig. 7(a, b)]. Notably, the exponent of this power law is notably high ($b \approx 11$). This observation resonates with prior research, confirming the characteristic behavior of integrable and nonintegrable systems [17, 25, 31].

As we carried out our calculations while varying the system size N , we encountered an intriguing consistency:

the growth of the OTOC remained remarkably stable. Within the dynamics regime, these growth patterns consistently remained parallel to each other across different system sizes [Fig. 7(c)].

In both integrable and nonintegrable systems, the dynamic region of the OTOC demonstrates power-law growth. However, we find that the dynamic region is unable to effectively discriminate between integrable and chaotic systems. As a result, we shifted our focus to the saturation behavior of the OTOC. In the context of integrable Floquet systems, the saturation behavior of OTOCs exhibits a unique characteristic—oscillation. Specifically, the OTOCs display an asymmetric rise and fall within the saturation regime. Conversely, the nonintegrable Floquet systems paint a different picture. Here, the saturation behavior of OTOCs is marked by exact saturation. Unlike the oscillatory behavior seen in integrable systems, the chaotic systems tend to settle into a fixed state at saturation, reflecting the chaotic nature of their dynamics. The intriguing aspect of our investigation lies in the consistency of this behavior across different Floquet periods. Whether we examine the systems at one, two, or even three Floquet periods $\tau = \pi/16$ [Fig. 8(a)], $\tau = \pi/6$ [Fig. 8(b)], and $\tau = \pi/4$ [Fig. 8(c)], the behavior remains remarkably similar. In our observations, the value of $C(n)/C(\infty)$ falls within the range of 0 to 2 due to the bounded nature of the asymptotic value of $C_4(n)/C(\infty)$, which remains between -1 and 1 during the post-scrambling phase. Furthermore, the asymptotic value of $C_2(n)/C(\infty)$ converges to 1.

We calculate NNSD for both integrable and nonintegrable periodic quenched field Floquet systems with a period of $\tau = \pi/4$. The integrable realm presents us with a consistent observation: Poisson-type behavior in spectral statistics across all numbers of kicks. This consistent pattern reflects an integrable characteristic of the system throughout the time evolution of the system [Fig. 9(a–f)]. However, the nonintegrable domain displays a different picture. Initially, the spectral statistics mimic Poisson-type behavior for a certain number of initial kicks. This behavior speaks to the presence of localized modes and partial regularity in the evolution of the system. However, after a distinct number of kicks, a shift occurs to Wigner-Dyson-type behavior, signifying the emergence of chaotic and globally randomized dynamics [Fig. 9(g–l)]. This transition indicates that the system undergoes a transition to chaos after a certain number of kicks. Contrary to the behavior observed in the linear quenched field Floquet system, in the periodic quenched field Floquet system, the system displays a different pattern in the NNSD. In the linear quenched field case, the system transitions to Wigner-Dyson behavior in the early stages of the evolution, occurring after just a few kicks. This is because the longitudinal field is fixed, while the transverse field starts with an initial small value h_{x0} . This setup initiates a competition between the longitudinal and transverse fields in the initial time regimes. In contrast, with a periodic quenched field,

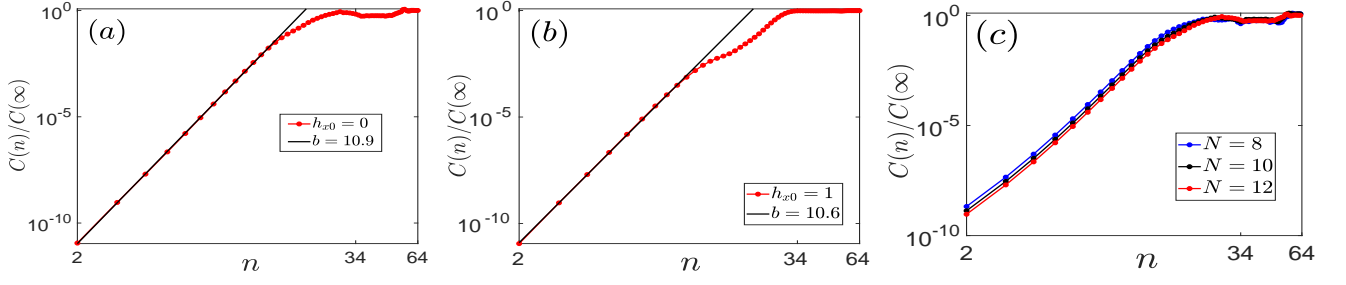


FIG. 7: $C(n)/C(\infty)$ using SBO vs. n (log – log) for (a) integrable $\hat{\mathcal{U}}_{0p}$ and (b) nonintegrable $\hat{\mathcal{U}}_{xp}$ system ($h_{x0} = 1$) with system size $N = 12$. (c) $C(n)/C(\infty)$ using SBO vs. n (log – log) for integrable $\hat{\mathcal{U}}_{0p}$ with system size $N = 8, 10$, and 12 . Other parameters are: $J = 1$, $h_z = 4$, $t_{\max} = 8\pi$, $\tau = \pi/4$, and $\alpha = \pi/2t_{\max}$. Open boundary conditions are considered.

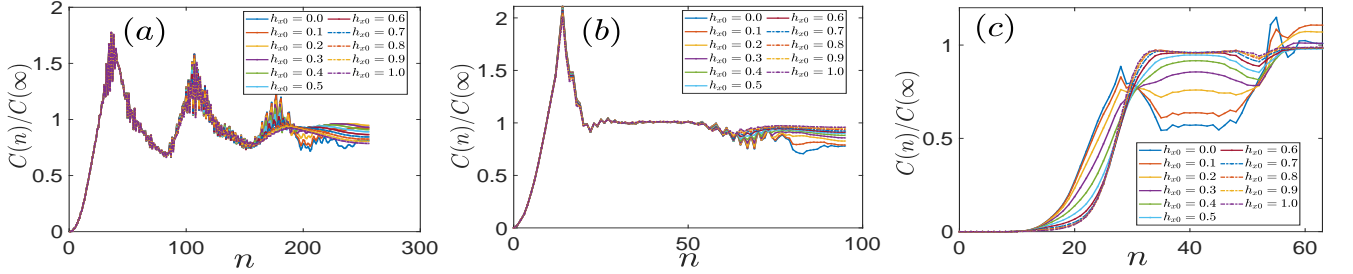


FIG. 8: $C(n)/C(\infty)$ vs n for different value of h_{x0} lies in between 0 to 1 differing by 0.1 for nonintegrable $\hat{\mathcal{U}}_{xp}$ system at period (a) $\tau = \pi/16$, (b) $\tau = \pi/6$, and (c) $\tau = \pi/4$. Other parameters are: $J = 1$, $h_{z0} = 4$, $t_{\max} = 16\pi$, $\alpha = \pi/2t_{\max}$, and system size $N = 12$. Open boundary conditions are considered.

the system shows Wigner-Dyson behavior after some additional kicks. Here, the longitudinal field starts from zero, and the transverse field starts from a high value of $h_x = 4$. Initially, the transverse field dominates over the longitudinal field. However, as time progresses, the transverse field decreases due to its cosine form, while the longitudinal field increases due to its sine form. After some kicks, the effect of the longitudinal field becomes significant in determining the NNSD.

Subsequently, we extended our study to consider localized Pauli spin observables in the x-direction at positions 1 and $N/2$, *i.e.*, $\hat{W} = \hat{\sigma}_1^x$ and $\hat{V} = \hat{\sigma}_{N/2}^x$. In calculating the OTOC for a localized observable, we focus on the operator C_4 because C_2 can be simplified to the identity operator due to the unitarity of Pauli observables. Consequently, in the limit as n approaches infinity, C_4 tends toward the identity, *i.e.*, $C_4 \rightarrow 1$ [25]. Therefore, when calculating $C(n)$, it is not necessary to divide by $C(\infty)$. Remarkably, we found consistent saturation behavior of the OTOCs similar to what we observed with the block spin observables. In the integrable case, the OTOCs exhibited oscillating saturation behavior, while in the chaotic case, we again observed exact saturation behavior at different time periods: $\tau = \pi/16$, $\tau = \pi/6$, and $\tau = \pi/4$ [Fig. 10 (a – c)].

Appendix B: OTOCs using SBOs and Pauli observables with z -direction alignment in periodic quenched field Floquet systems

Since the behavior of the OTOC depends on the choice of observables, it is crucial to analyze OTOC with different observables to establish the saturation region as a universal discriminator. To this end, we define SBOs aligned in the z -direction as $\hat{W} = \sum_{i=1}^{N/2} \hat{S}_i^z$ and $\hat{V} = \sum_{i=N/2+1}^N \hat{S}_i^z$. Our investigations cover both integrable and nonintegrable systems under the influence of the operator $\hat{\mathcal{U}}_{xp}$. For the OTOC calculations, we consider three periods: $\tau = \pi/16$, $\tau = \pi/6$, and $\tau = \pi/4$. In all cases, we observe the oscillatory behavior of the OTOC in the integrable case, while in the chaotic case, we observe exact saturation behavior [see Fig. 11 (a – c)]. When the period is short, the saturation regime of the OTOC shows an increasing trend, indicating incomplete thermalization [see Fig. 11 (a)]. However, compared to the integrable case, we observe a non-oscillating behavior in the chaotic case. As the period increases, for large amplitudes of the longitudinal field (around 1), we observe exact saturation [see Fig. 11 (b,c)]. This suggests that when the longitudinal field is comparable to the transverse field, the system undergoes thermalization.

Finally, we considered localized Pauli spin observables in the z -direction at positions 1 and $N/2$, *i.e.*, $\hat{W} = \hat{\sigma}_1^z$

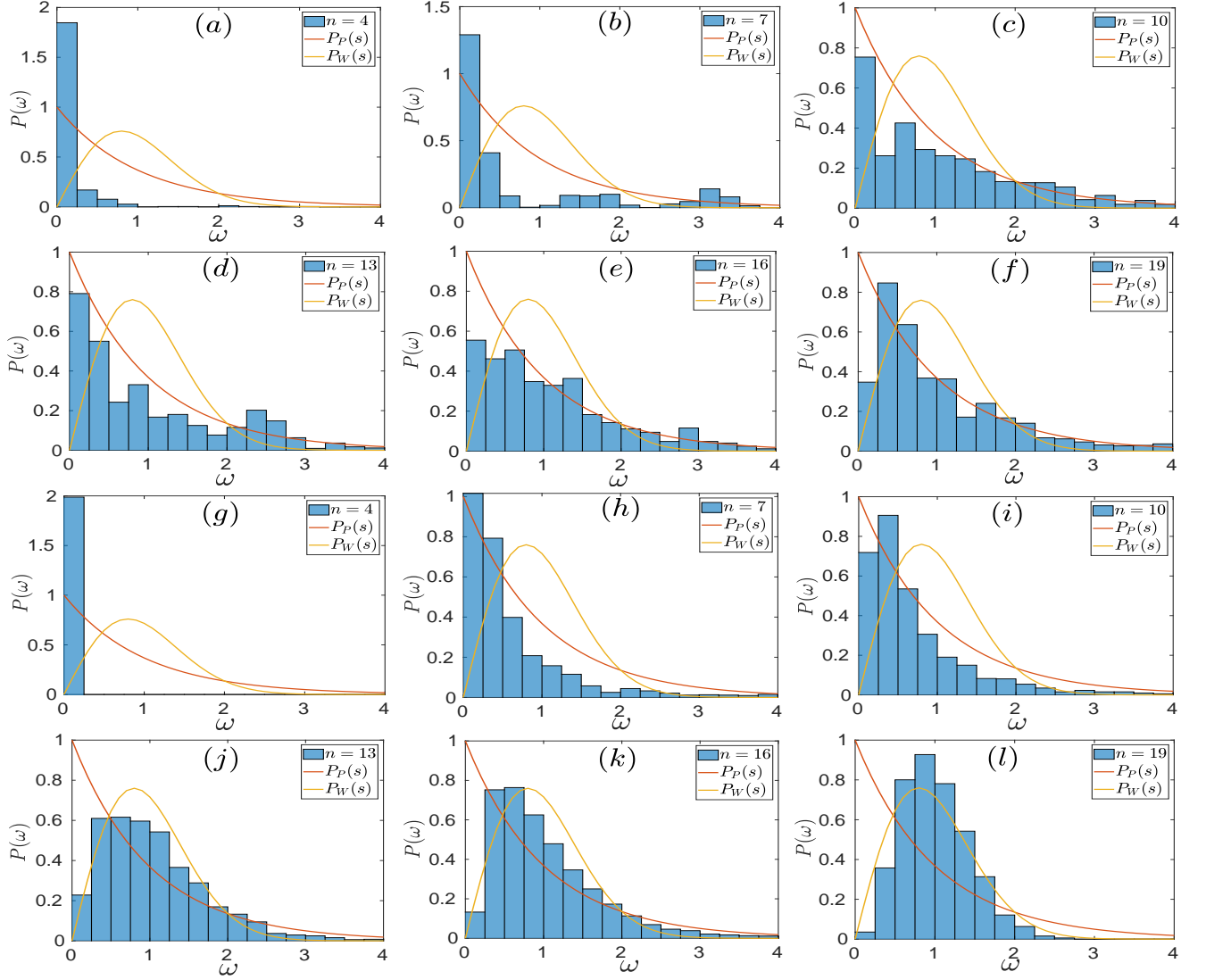


FIG. 9: NNSD of the (a – f) integrable $\hat{\mathcal{U}}_{0p}$ system, and (g – l) nonintegrable $\hat{\mathcal{U}}_{xp}$ system at period $\tau = \pi/4$ in the even Palindromic space at different kicks mentioned in the legend. Other parameters are: $\alpha = \pi/2t_{\max}$, and $t_{\max} = 16\pi$, $J = 1$, $h_{x0} = 0/4$, $h_{z0} = 4$, $N = 12$. Open boundary conditions are considered.

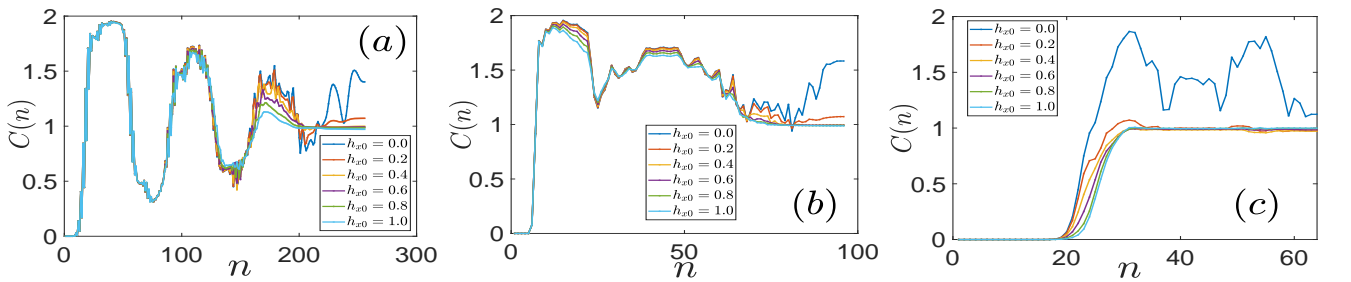


FIG. 10: $C(n)$ ($\hat{W} = \hat{S}_1^x$, and $\hat{V} = \hat{S}_{N/2}^x$) vs n for different value of h_{x0} lies in between 0 to 1 differing by 0.1 for nonintegrable $\hat{\mathcal{U}}_{xp}$ system at period (a) $\tau = \pi/16$, (b) $\tau = \pi/6$, and (c) $\tau = \pi/4$. Other parameters are: $J = 1$, $h_{z0} = 4$, $t_{\max} = 16\pi$, $\alpha = \pi/2t_{\max}$, and system size $N = 12$. Open boundary conditions are considered.

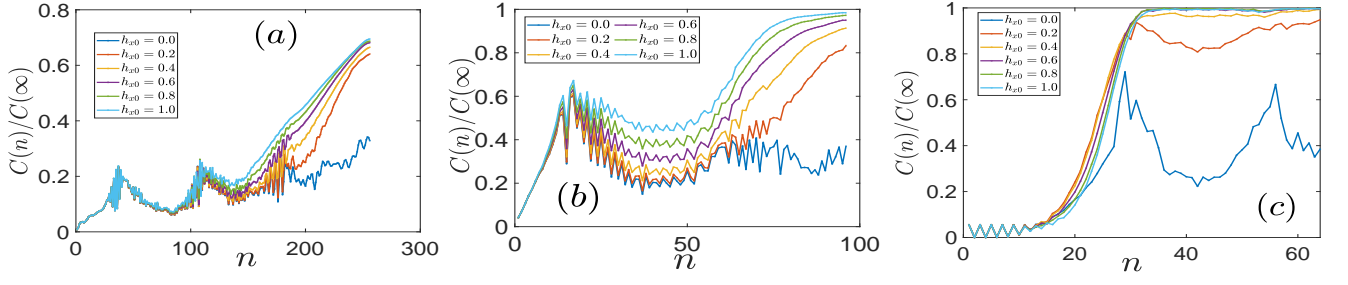


FIG. 11: $C(n)/C(\infty)$ ($\hat{W} = \sum_{i=1}^{N/2} \hat{S}_i^z$, and $\hat{V} = \sum_{i=N/2+1}^N \hat{S}_i^z$) vs n for different value of h_{x0} lies in between 0 to 1 differing by 0.2 for nonintegrable $\hat{\mathcal{U}}_{xp}$ system at period (a) $\tau = \pi/16$, (b) $\tau = \pi/6$, and (c) $\tau = \pi/4$. Other parameters are: $J = 1$, $h_{z0} = 4$, $t_{\max} = 16\pi$, $\alpha = \pi/2t_{\max}$, and system size $N = 12$. Open boundary conditions are considered.

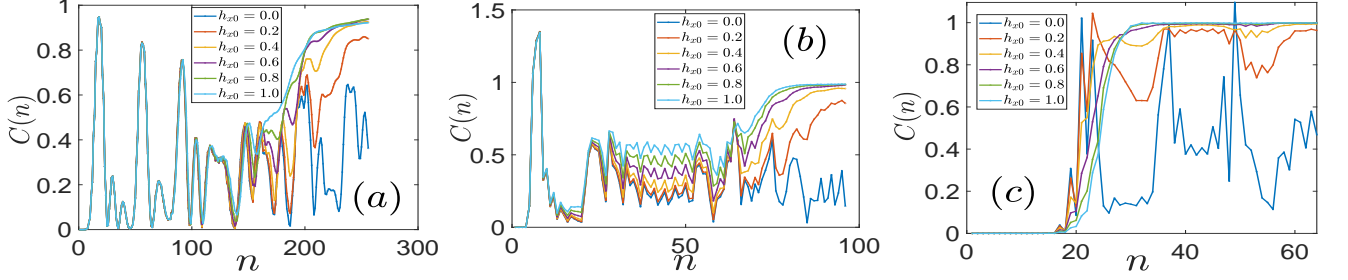


FIG. 12: $C(n)$ ($\hat{W} = \hat{S}_1^z$, and $\hat{V} = \hat{S}_{N/2}^z$) vs n for different value of h_{x0} lies in between 0 to 1 differing by 0.1 for nonintegrable $\hat{\mathcal{U}}_{xp}$ system at period (a) $\tau = \pi/16$, (b) $\tau = \pi/6$, and (c) $\tau = \pi/4$. Other parameters are: $J = 1$, $h_{z0} = 4$, $t_{\max} = 16\pi$, $\alpha = \pi/2t_{\max}$, and system size $N = 12$. Open boundary conditions are considered.

and $\hat{V} = \hat{\sigma}_{N/2}^z$. Much like the previous cases, we found consistent saturation behavior of the OTOCs, resembling the behavior seen with the block spin observables. In the

integrable case, the OTOCs displayed oscillating saturation behavior, while in the chaotic case, we again observed exact saturation behavior at different time periods: $\tau = \pi/16$, $\tau = \pi/6$, and $\tau = \pi/4$ [Fig. 12 (a – c)].